



Miguel Alexandre Branco Tibério

Bachelor in Science of Micro and Nanotechnologies Engineering

Study of localized transport phenomena of Cu_2O

Dissertation submitted in partial fulfillment of the requirements for the degree of
Master of Science in

Micro and Nanotechnologies Engineering

Supervisor: Dr. Jonas Deuermeier, Postdoctoral Researcher, Faculdade de
Ciências e Tecnologia, Universidade Nova de Lisboa

Co-supervisor: Dr. Suman Nandy, Postdoctoral Researcher, Faculdade de
Ciências e Tecnologia, Universidade Nova de Lisboa



FACULDADE DE
CIÊNCIAS E TECNOLOGIA
UNIVERSIDADE NOVA DE LISBOA

October 2019

Study of localized transport phenomena of Cu₂O

Copyright © Miguel Alexandre Branco Tibério, Faculdade de Ciências e Tecnologia, Universidade Nova de Lisboa.

Faculdade de Ciências e Tecnologia and Universidade Nova de Lisboa have the right, perpetual and without geographical boundaries, to file and publish this dissertation through printed copies reproduced on paper or on digital form, or by any other means known or that may be invented, and to disseminate through scientific repositories and admit its copying and distribution for non-commercial, educational or research purposes, as long as credit is given to the author and editor.

Aos que estão no meu coração.

Acknowledgements

First of all, I would like to thank Dr. Jonas Deuermeier for guiding me through all this process. You've always been very helpful and kind, and I appreciate all the time you spent with me. You really contributed for making this experience better. I need to thank Dr. Suman Nandy as well for his help. I won't forget that time at the lab where I learned more about the sacrifices you made to be where you are now. Tomás Calmeiro also deserves a huge acknowledgement for all the effort he put on the AFM measurements. You definitely made this work a lot richer and those silent times on the lab funnier. I would also like to thank Prof. Dr. Daniela Nunes for making the SEM measurements, and to Alexandra Gonçalves and Sónia Pereira for the help they provided me in the lab.

Agradeço ao André, o meu padrinho, por me ter acompanhado durante o meu percurso académico. Obrigado por todas as conversas que nos tornaram amigos. Obrigado também por teres feito os dias passarem mais rápido e por me teres evitado algumas viagens à faculdade. À Filipa e ao Miguel, obrigado por terem tornado o meu percurso académico sem dúvida mais feliz.

Aos meus amigos de sempre e para sempre: Ana, Castelo, Filipa, João, Mel e Tiago. Obrigado por me darem tantas alegrias, gargalhadas, conforto. Obrigado pelas viagens e pelas histórias. Obrigado por estarem aqui, especialmente quando é mais difícil. Ao Dan, um agradecimento duplo por ser um apoio dentro e fora da faculdade. Ao Rodrigo, o amigo que podia ser irmão. Obrigado por me ensinares que, no jogo que é a vida, a amizade vence a distância.

Ao Nuno, que me deu o que eu mais precisava nesta fase: repreensões e amor. Um não se dissocia do outro, não é? Obrigado por tentares dar-me algum ânimo, mesmo quando parecia não ter efeito. Obrigado por me ouvires quando só me apetecia desistir. E obrigado por estares comigo, incondicionalmente.

Um obrigado especial aos que mais contribuíram para o meu crescimento e que me deram tanto, especialmente durante a infância: tia Olga, avó Bárbara, avô António, avó Amélia. Aos meus pais, um obrigado pelos avisos sucessivos sobre o prazo de entrega da tese. Acho que já o decorei. Agora mais a sério, obrigado pela preocupação. E obrigado pelo investimento que fizeram em mim ao longo destes anos. Apesar de às vezes não parecer, tenho noção de que não há investimento mais bonito e altruísta do que aquele que se faz num filho. Espero, um dia, vir a investir assim em alguém.

Abstract

Cu₂O is a p-type semiconductor with a wide range of applications in optoelectronics, namely solar cells. Performance limitations have been previously ascribed to an inhomogeneous local conductivity: notably highly conductive grain boundaries compared to the grains. In this work, polycrystalline Cu₂O thin-films fabricated by reactive sputter deposition were studied. In addition, Cu₂O particles with cubic and octahedral shapes were produced from solution. The facets of cubic particles have a (100) orientation, whereas octahedral particles have facets with (111) orientation. Electrical modes of atomic force microscopy were used to study the localized transport mechanisms of the differently prepared Cu₂O samples. Remarkably, the thin-film Cu₂O samples of this work all showed more conductive grains compared to the grain boundaries. The results were analyzed in conjunction with structural, chemical, optical and morphological information.

Keywords: local conductivity; grain boundaries; facets; conductive atomic force microscopy; Cu₂O; reactive sputtering.

Resumo

O Cu_2O é um semicondutor tipo-p com uma vasta gama de aplicações, nomeadamente células solares. Algumas limitações de desempenho têm sido atribuídas a uma condutividade local não-homogénea: fronteiras de grão altamente condutoras comparativamente aos grãos. Neste trabalho, foram estudados filmes-finos de Cu_2O policristalino fabricados por *sputtering* reativo. Para além disso, foram produzidas partículas de Cu_2O com formas cúbicas e octaédricas através de solução. As faces das partículas cúbicas têm uma orientação (100), enquanto as partículas octaédricas têm faces com orientação (111). De forma a estudar os mecanismos de transporte localizados das diferentes amostras de Cu_2O preparadas, foram utilizados modos elétricos de microscopia de força atómica. Curiosamente, todos os filmes-finos de Cu_2O produzidos no decorrer deste trabalho mostraram ter grãos mais condutores comparativamente às fronteiras de grão. Os resultados foram analisados em conjunto com informação estrutural, química, ótica e morfológica.

Palavras-Chave: condutividade local; fronteiras de grão; faces; microscopia de força atómica condutora; Cu_2O ; *sputtering* reativo.

Contents

1. INTRODUCTION	1
2. EXPERIMENTAL PROCEDURE	3
2.1. Cu_2O THIN-FILM DEPOSITION	3
2.2. Cu_2O PARTICLE SYNTHESIS	4
2.3. CHARACTERIZATION TECHNIQUES	5
3. RESULTS AND DISCUSSION	9
3.1. THIN-FILMS	9
3.1.1. TRANSMITTANCE SPECTROSCOPY	9
3.1.2. X-RAY DIFFRACTION	11
3.1.3. SCANNING ELECTRON MICROSCOPY	14
3.1.4. X-RAY PHOTOELECTRON SPECTROSCOPY	15
3.1.5. ATOMIC FORCE MICROSCOPY AND CONDUCTIVITY MEASUREMENTS	16
3.2. PARTICLES	23
3.2.1. SCANNING ELECTRON MICROSCOPY	23
3.2.2. X-RAY DIFFRACTION	25
3.2.3. ENERGY DISPERSIVE X-RAY SPECTROSCOPY	25
3.2.4. ATOMIC FORCE MICROSCOPY	26
4. CONCLUSIONS AND FUTURE PERSPECTIVES	29
REFERENCES	31
ANNEXES	33
ANNEX A	33
ANNEX B	34
ANNEX C	34
ANNEX D	34

List of Figures

Figure 2.1 – (a) LP, (b) HP and (c) LP-SB sets of Cu ₂ O thin-films. These thin-films were deposited on ITO-coated glass and they are organized, from left to right, by an increasing O ₂ flow rate.	4
Figure 2.2 – (a) Cu ₂ O thin-films deposited on three different substrates (top-right: corning glass; top-left: ITO-coated glass; bottom: silicon); (b) Cu ₂ O particles prepared by two different methods (left: powder on carbon tape; drop-casted films).....	6
Figure 3.1 – Tauc plots of (a) LP, (b) HP and (c) LP-SB sets of Cu ₂ O thin-films, consisting of four LP samples, five HP samples and three LP-SB samples deposited using different O ₂ flow rates.	10
Figure 3.2 – XRD results of the LP set of Cu ₂ O thin-films, consisting of four samples deposited using different O ₂ flow rates. The main peaks of Cu ₂ O are represented by the dashed lines.	11
Figure 3.3 – XRD database references of copper oxides (Cu ₂ O, CuO and Cu ₄ O ₃) and metallic Cu.....	12
Figure 3.4 – XRD results of the most stoichiometric Cu ₂ O thin-films from each set (LP-SB, LP and HP), including HP-heated film. The main peaks of Cu ₂ O are represented by the dashed lines.....	13
Figure 3.5 – XRD results of two Cu ₂ O thin-films from the HP set, deposited using 0.7 sccm and 0.8 sccm O ₂ flow rates. The main peaks of Cu ₂ O are represented by the dashed lines.	14
Figure 3.6 – SEM cross-sectional image of the most stoichiometric LP Cu ₂ O thin-film deposited on a silicon substrate.	15
Figure 3.7 – XPS data from (a) Cu 2p and (b) O 1s emissions relative to the LP set of films, consisting of four samples deposited using different O ₂ flow rates.	15
Figure 3.8 – Mask applied by Gwyddion software. The I _G was measured outside the mask.	16
Figure 3.9 – Topographic images and respective current maps of every Cu ₂ O thin-film from the LP set, consisting of four samples deposited using different O ₂ flow rates: (a) 1.1 sccm, (b) 1.2 sccm, (c) 1.3 sccm and (d) 1.4 sccm.	17
Figure 3.10 – Topographic images and respective current maps of the most stoichiometric Cu ₂ O thin-films from each set: (a) LP-SB, (b) LP and (c) HP, including (d) HP-heated film.	18
Figure 3.11 – Topographic images and respective current maps of Cu ₂ O thin-films deposited under the same conditions as the most stoichiometric film from the LP set, consisting of four	

samples deposited during different times: (a) 7.5 minutes, (b) 15 minutes, (c) 30 minutes and (d) 60 minutes.....	20
Figure 3.12 – Topographic images and respective current maps of Cu ₂ O thin-films from the HP set with different preferential orientations, consisting of two samples deposited using different O ₂ flow rates: (a) 0.7 sccm and (b) 0.8 sccm.....	21
Figure 3.13 – (a) Topographic image and (b) respective current map of the LP film deposited using a 1.1 sccm O ₂ flow rate. The top half of either image was obtained by using a -2 V voltage and the bottom half using a +2 V voltage.	22
Figure 3.14 – (a) Topographic image and (b) respective current map of the most stoichiometric Cu ₂ O thin-film from the HP set obtained by <i>Cypher S</i>	23
Figure 3.15 – SEM images of (a) cubic and (b) octahedral particles obtained in the 1 st synthesis.	24
Figure 3.16 – SEM images of (a) cubic and (b) octahedral particles obtained in the 2 nd synthesis.	24
Figure 3.17 – XRD results from cubic and octahedral particles obtained in the 1 st synthesis. The main peaks of Cu ₂ O are represented by the dashed lines.....	25
Figure 3.18 – (a) Topographic image and (b) respective current map of unoptimized octahedral particles obtained by a <i>Cypher S</i> system.	26
Figure 3.19 – (a) Topographic image and (b) respective current map of octahedral particles from the 1 st synthesis obtained by a <i>MFP-3D-SA</i> system.....	27
Figure 3.20 – Topographic images and respective resistivity maps of (a) cubic and (b) octahedral particles from the 1 st synthesis. Images obtained by a <i>Nano-Observer</i> system.....	27

List of Tables

Table 2.1 – Parameters used in the sputter deposition of the three sets of Cu ₂ O thin-films: LP, HP and LP-SB.	3
Table 2.2 – Summary of the characterization techniques used to analyze the Cu ₂ O structures produced (films and particles), organized by the type of properties provided.	5
Table 3.1 – Most stoichiometric Cu ₂ O thin-films from each set (LP, HP and LP-SB) and respective bandgaps.....	10
Table 3.2 – I_G , σ_{OOP-G} and σ_{IP} of every Cu ₂ O thin-film from the LP set, consisting of four samples deposited using different O ₂ flow rates.....	18
Table 3.3 – I_G , σ_{OOP-G} and σ_{IP} of the most stoichiometric Cu ₂ O thin-films from each set, including HP-heated film.	19
Table 3.4 – I_G , σ_{OOP-G} and σ_{IP} of Cu ₂ O thin-films deposited under the conditions of the most stoichiometric film from the LP set, consisting of four samples deposited during different times.	20
Table 3.5 – I_G , σ_{OOP-G} and σ_{IP} of Cu ₂ O thin-films from the HP set with different preferential orientations, consisting of two samples deposited using different O ₂ flow rates.	21
Table 3.6 – Oxygen content of cubic and octahedral particles from both syntheses, obtained by EDS.....	25

List of Abbreviations

AFM	atomic force microscopy
α	absorption coefficient
A_{tip}	area of the bigger AFM tip cross-section
CAFM	conductive atomic force microscopy
d	distance between consecutive crystallographic planes
EDS	energy-dispersive X-ray spectroscopy
HP	higher pressure
ICDD	International Centre for Diffraction Data
I_G	average grain current
IPA	isopropyl alcohol
ITO	indium tin oxide
KPFM	Kelvin probe force microscopy
λ	wavelength
LP	lower pressure
LP-SB	lower pressure with substrate bias
PDF	Powder Diffraction File
PVP	polyvinylpyrrolidone
R	reflectance
RF	radio-frequency
SEM	scanning electron microscopy
σ_{IP}	in-plane conductivity of a film
$\sigma_{\text{OOP-G}}$	out-of-plane conductivity of the grains
T	transmittance
t_{film}	film thickness
θ	glancing angle
V_{CAFM}	voltage used during CAFM measurements
XPS	X-ray photoelectron spectroscopy
XRD	X-ray diffraction

1.Introduction

Nowadays, characteristics like flexibility and transparency are becoming almost mandatory relatively to electronic devices. While n-type transparent oxide semiconductors are being developed with great results, p-type ones are facing several difficulties related to performance. Metal oxides like NiO and SnO are being studied with the purpose to fill that gap, although cuprous oxide is one of the big candidates. In the form of a thin-film, it has great potential due to its 2.17 eV bandgap (which makes it semi-transparent) and to the possibility of being prepared at low temperature (allowing its deposition on flexible substrates). Besides that, it is abundant in nature, non-toxic and it has a low production cost. [1]

Despite all the advantages of using Cu_2O , its implementation on p-type thin-film transistors (TFTs), complementary metal-oxide-semiconductor (CMOS) devices and solar cells is limited due to some performance drawbacks. Unlike Cu_2O in bulk form, Cu_2O TFTs are demonstrating a high conductivity in the off-state and a low field-effect mobility, which makes the devices unfunctional. [2] It is known that the polycrystalline structure of the Cu_2O thin-films is in the center of the problem, which is aggravated when Cu_2O is deposited at low temperatures since the grains become smaller. [3]

It is reported that Cu_2O grain boundaries are mainly formed by CuO, with a higher conductivity, which masks the current rectification properties from the Cu_2O grains. [2], [4] Besides that, grain boundaries act as shunt paths, affecting carrier mobility. [5]

Cu_2O can be deposited by different techniques, namely, sputtering, pulsed laser deposition, molecular beam epitaxy, chemical vapor deposition and electrochemical deposition. [3] In this work, Cu_2O thin-films were produced by reactive sputter deposition. The main goal was to reproduce the behavior described above in which the grain boundaries were more conductive than the grains. To observe that, atomic force microscopy (AFM) and one of its electrical modes, conductive atomic force microscopy (CAFM), were intensely used, as in other works. [5], [6] After altering the deposition parameters several times and even performing post-deposition heating treatments on the films, the opposite situation was constantly observed: the grains were more conductive than the grain boundaries. This behavior was not yet reported.

Previously, some differences in electrical behavior of the films were ascribed to metallic precipitates inside Cu_2O . [7] However, the facets of grain interfaces present in the films can also have influence. Several facet-dependent behaviors on Cu_2O have been studied. For example: (111)-textured films have higher carrier mobility [8]; photocatalytic activity is described as higher in the

(111) direction compared to (100) oriented facets [9]; CAFM shows that the conductivity of an octahedral particle is different along one of its (111) facets [10]; electrical conductivity is reported to be higher between (111) facets of an octahedral particle than between (100) facets of a cubic particle. [11]

Although it is not simple to control the facet orientation of grains in a film, particles allow that kind of control. [12], [13] In this work, Cu_2O particles were produced from solution in two different shapes: cubic particles with (100) facets and octahedral particles with (111) facets.

2. Experimental Procedure

2.1. Cu₂O Thin-film Deposition

The deposition of the Cu₂O thin-films was made by reactive radio-frequency (RF) magnetron sputtering and the system used was an *ATC-Orion 8 UHV* from *AJA International*. It was used a 2 inch (5.08 cm diameter) copper target with a 99.99% purity from *Plasmaterials*.

To allow the thin-film characterization by different techniques, the films were deposited on three different substrates: corning glass, indium tin oxide (ITO)-coated corning glass and silicon. These substrates were previously cleaned in an ultrasound bath with acetone, followed by isopropyl alcohol (IPA), for 10 minutes each. Then, the films were washed with deionized water and dried with compressed nitrogen.

The first depositions were not resulting in uniform films, so an adjusting of the magnetron tilting was required (0.95° was the optimized value). After that, several parameters were kept constant, while others were altered to understand their influence on the films. All these parameters are presented in Table 2.1. The films were deposited under three different main conditions: lower pressure (LP), higher pressure (HP) and lower pressure with substrate bias (LP-SB). LP set of films was the first to be deposited. Depositing under HP and LP-SB conditions would theoretically result, respectively, in less dense and denser films. That could be interesting to understand if the film density would influence other properties of the films, namely, structural and electrical.

Table 2.1 – Parameters used in the sputter deposition of the three sets of Cu₂O thin-films: LP, HP and LP-SB.

	LP	HP	LP-SB
Total Pressure (Pa)	0.2	0.4	0.2
Ar flow rate (sccm)	18		
O₂ flow rate (sccm)	1.1; 1.2; 1.3; 1.4	0.6; 0.7; 0.8; 0.9; 1.0	1.1; 1.2; 1.3
RF power (W)	60		
Substrate Bias (W)	-	-	15
Pre-sputtering Time (min)	10		
Deposition Time (min)	60		

All the depositions occurred at room temperature and with the maximum level of substrate rotation set on. Parameters like RF power and deposition time were also kept constant among the three sets of films. The 10 minutes of pre-sputtering are important to make sure that, when a deposition starts, the conditions of the target surface have stabilized. The goal was to deposit Cu_2O thin-films, so an ideal Cu/O ratio of 2:1 had to be achieved. Knowing that a Cu_2O film has a yellowish color, the Ar flow rate was kept constant while the O_2 flow rate was adjusted by observing the color of the films obtained. The three sets of films are displayed in Figure 2.1.

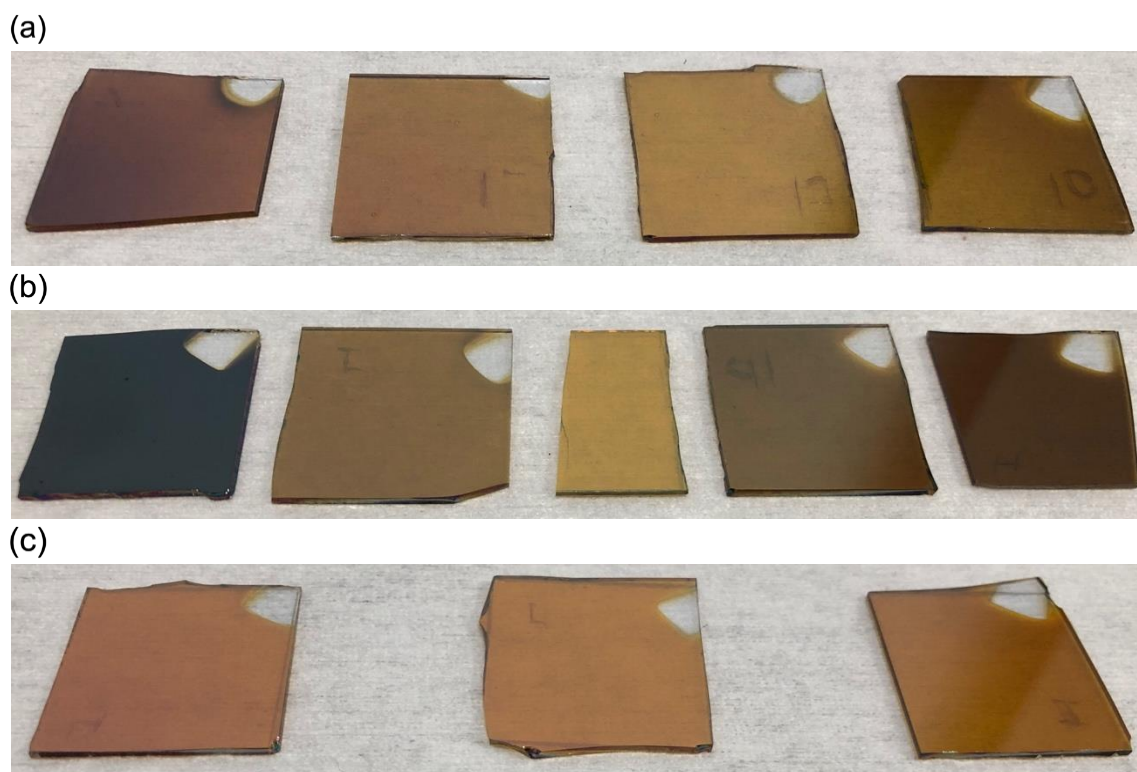


Figure 2.1 – (a) LP, (b) HP and (c) LP-SB sets of Cu_2O thin-films. These thin-films were deposited on ITO-coated glass and they are organized, from left to right, by an increasing O_2 flow rate.

To understand the possible influence of film thickness on other film properties, thinner films were deposited in LP conditions by halving the deposition time successively (30 min; 15 min; 7.5 min). Also, to verify the influence of oxidizing the films by temperature, the most stoichiometric film from the HP set was later heated for 24 hours at 100 °C in a post-deposition treatment.

2.2. Cu_2O Particle Synthesis

The synthesis of the Cu_2O particles was based on a published article. [13] To investigate the influence of the particle shape on other properties, cubic and octahedral particles have been made by the same solution-based method. The particles have been made simultaneously, in different containers. The synthesis of either shape of particles only differs in a single step, which will be highlighted. The quantities present in the following procedure refer to a single container where

will occur a synthesis of a specific particle shape. The quantities are the same for the other container.

First of all, 100 mL of a $\text{CuCl}_2 \cdot 2\text{H}_2\text{O}$ aqueous solution (0.01 M) were prepared. To obtain octahedral particles, 3.334 g of polyvinylpyrrolidone (PVP), with a weight average molecular weight of 10 000 g/mol, was added to the previous solution. No PVP was added to the synthesis of the cubic particles. Then, 10 mL of a NaOH aqueous solution (2 M) was added dropwise, followed by 30 minutes of waiting. After that, 10 mL of an ascorbic acid aqueous solution (0.6 M) was added, also dropwise, followed by 3 hours of waiting. The whole process occurred under constant stirring and in a 55 °C water bath. The solution was then centrifuged (6000 rpm, 15 minutes) and decanted. The resulting precipitate was washed 3 times with distilled water and twice with ethanol (6000 rpm, 10 minutes each). In the end, the precipitate was dried at room temperature, resulting in a powder.

2.3. Characterization Techniques

Several characterization techniques were used to analyze the Cu_2O structures produced: profilometry, transmittance spectroscopy, X-ray diffraction (XRD), scanning electron microscopy (SEM), energy-dispersive X-ray spectroscopy (EDS), X-ray photoelectron spectroscopy (XPS), resistivity measurements and atomic force microscopy (AFM), in conjunction with conductive atomic force microscopy (CAFM), one of its electrical modes. In Table 2.2, it is possible to observe which techniques were used to characterize either the films or the particles and the type of information they provide.

Table 2.2 – Summary of the characterization techniques used to analyze the Cu_2O structures produced (films and particles), organized by the type of properties provided.

Properties	Films	Particles
Morphological	Profilometry SEM (cross-section) AFM	SEM AFM
Structural	XRD	XRD
Optical	Transmittance Spectroscopy	-
Chemical	XPS	XPS EDS
Electrical	CAFM Conductivity measurements	CAFM

As mentioned before, the films were deposited on various substrates so they could be analyzed by the different techniques. The particles were also prepared in different ways to facilitate the characterization process. Figure 2.2 displays the films deposited on different substrates and

the particles prepared by different methods. Below, the details on each technique are explained, namely, the sample preparation involved, the equipment and the parameters used.

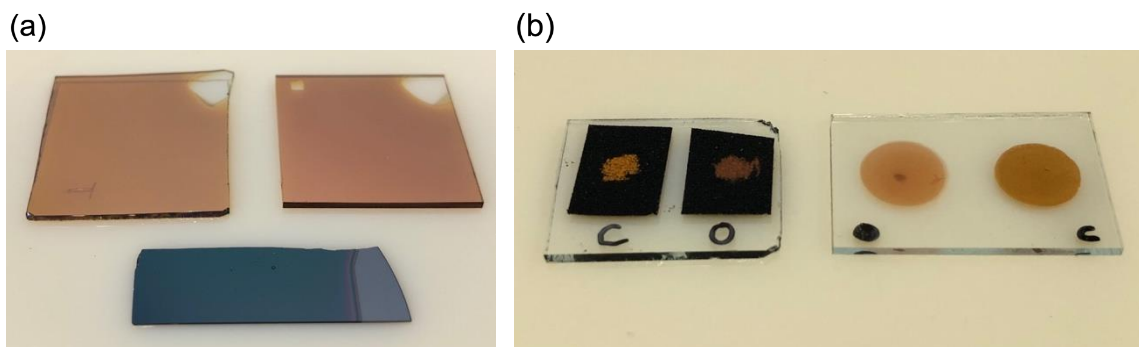


Figure 2.2 – (a) Cu₂O thin-films deposited on three different substrates (top-right: corning glass; top-left: ITO-coated glass; bottom: silicon); (b) Cu₂O particles prepared by two different methods (left: powder on carbon tape; drop-casted films).

Profilometry (*XP-200* from *Ambios*) was used to measure the thickness of the films. The measurements were made on the films deposited on glass since it is a relatively flat substrate.

Transmittance spectroscopy (*Lambda 950* from *PerkinElmer*) allowed obtaining optical information of the films, namely the optical bandgap. The films deposited on glass were analyzed since glass is transparent to a wide range of wavelengths.

XRD (*X'Pert PRO MRD* from *PANalytical*) provided structural information of both Cu₂O structures. Regarding the films, an amorphous substrate was needed, so the films deposited on glass were analyzed. The particle structure was verified by placing the powder directly into a suitable holder.

SEM (*Auriga CrossBeam* from *ZEISS*) allowed obtaining morphological information of both Cu₂O structures. To prevent any charge accumulation, SEM is a technique that requires substrates with conductive properties. For that reason, the films deposited on silicon were used. To obtain cross-sectional images, the films were manually broken prior to the measurement. The particles also required a specific preparation. The powder was transferred to a carbon tape which was previously fixed on an ITO-coated glass. The powder excess was then blown with compressed nitrogen. In addition, chemical information of the particles was obtained by EDS (*X 150* from *Nano-Analysis*) while in the SEM chamber.

XPS (*AXIS Supra* from *Kratos Analytical* with a monochromated Al K α X-ray source) was used to obtain chemical information from the surface of both Cu₂O structures. To prevent any charge accumulation, similarly to SEM, films deposited on ITO-coated glass were used. The films were analyzed with a 225 W X-ray power, no aperture and a 5 eV pass energy. The particle preparation used was the same as in SEM. The particles were analyzed with a 300 W X-ray power, a 110 μ m aperture and a 20 eV pass energy.

The conductivity of the films was also measured by the van der Pauw method with a Hall Effect measurement system (*HL5500* from *Nanometrics*). Before that, Au contacts (with a thin Ni layer as adhesion promoter) were deposited by electron beam evaporation (home-made apparatus). For this technique, the films deposited on glass were used.

AFM was used to collect topographical information from both Cu_2O structures, whereas CAFM, one of AFM electrical modes, allowed obtaining their local conductivity properties. CAFM requires a substrate with conductive properties, so the films deposited on ITO-coated glass were used. Most of AFM/CAFM measurements on the films were performed by an *MFP-3D-SA* system from *Asylum Research*. As AFM and CAFM are both contact mode techniques, a *Nanoworld CONTPt* probe ($f_0 = 13$ kHz, $k = 0.2$ N/m) was used. All CAFM images were obtained by applying -2 V to the ITO present on the substrate of the films. One of the measurements was executed by a *Cypher S* system, also from *Asylum Research*.

Regarding the particles, the same preparation used in SEM and XPS analysis was tested in the AFM/CAFM measurements. Nonetheless, and to prevent the powder to be dragged from the tape, a film was made from the particles by drop-casting. First, the powder was dispersed into distilled water with an ultrasonic probe. To improve the adhesion of the dispersion to the ITO-coated glass, circular spots were activated with a UV-ozone system. The dispersion was then dropped using a micropipette. The water evaporated at room temperature, forming circular films with the dried powder. By chronological order, the particles were analyzed using *Cypher S* and *MFP-3D-SA* systems from *Asylum Research* (drop-casted films) and using a *Nano-Observer* system from *Concept Scientific Instruments* (powder on carbon tape).

All the AFM/CAFM images were analyzed using *Gwyddion* software.

3. Results and Discussion

3.1. Thin-films

3.1.1. Transmittance Spectroscopy

After depositing thin-films with different Cu/O ratios, transmittance spectroscopy was used. Since copper-containing materials can be distinguish by their absorption behaviors, this was the first technique to be used to verify which conditions lead to the formation of Cu₂O. [14] In the case of copper oxides (Cu₂O, CuO, Cu₃O₄), Cu₂O is the one with the highest bandgap, i.e., it starts absorbing at higher energies. In addition, contributions of metallic copper in Cu₂O would lead to an increased absorption at lower energies, compared to pure Cu₂O. [15]

To verify these differences, the absorption coefficient (α) was calculated from the transmittance data by Lambert-Beer law (1). The reflectance (R) was neglected since it only has a significant contribution on sub-bandgap absorption features. Only transmittance (T) was considered.

$$\alpha = \frac{\ln\left(\frac{T}{1-R}\right)}{t_{\text{film}}} \quad (1)$$

In the formula, t_{film} represents the thickness of the films which was previously measured by the profilometer. The average thickness of the films was 265 nm, later confirmed by SEM measurements. Finally, a Tauc plot was made for each set of Cu₂O thin-films (LP, HP and LP-SB). The most stoichiometric Cu₂O thin-film from each set corresponds to the sample that starts absorbing at higher energies. The bandgap of the most stoichiometric films was then determined by extrapolating the linear zone of the plot, as represented in Figure 3.1.

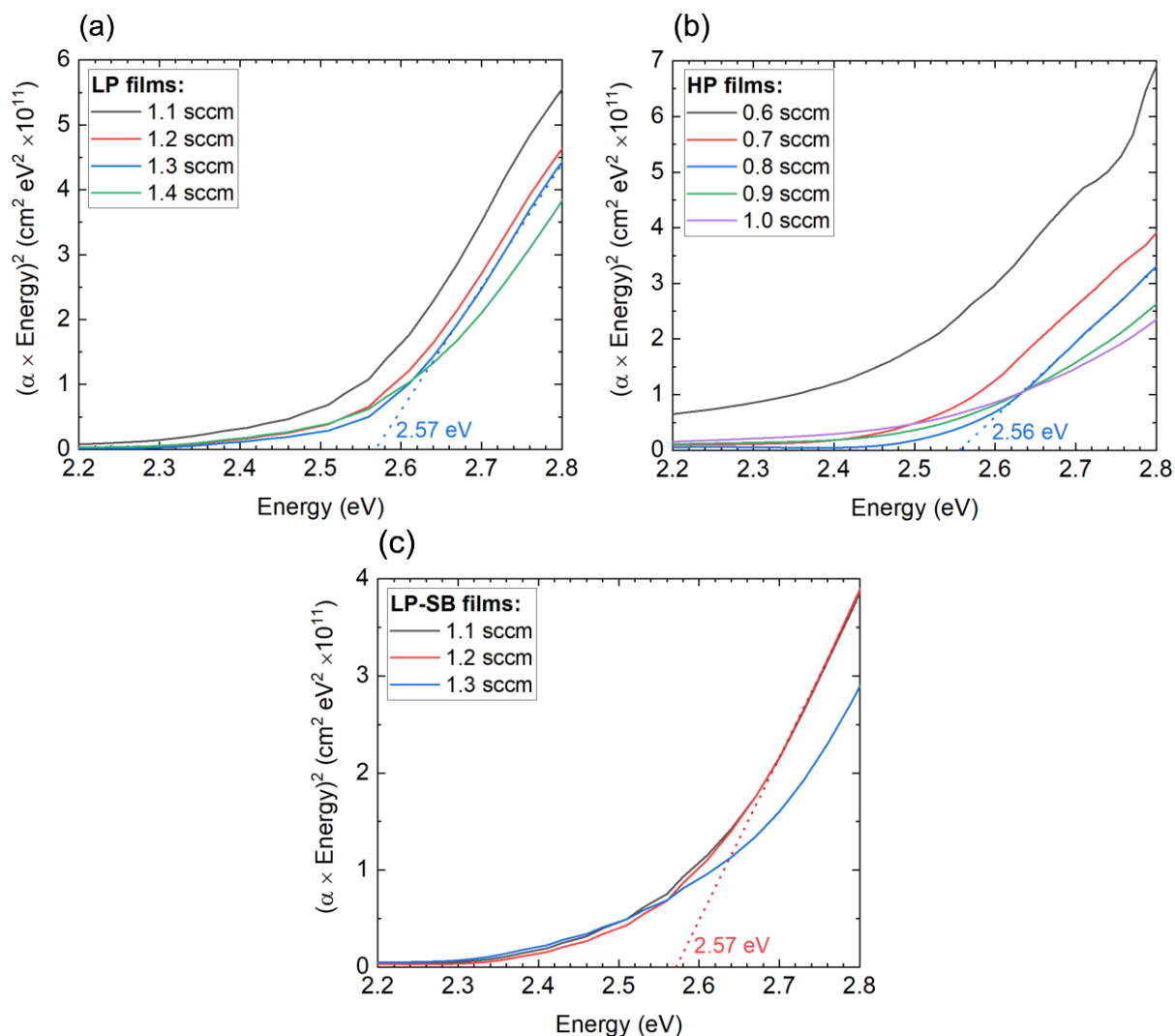


Figure 3.1 – Tauc plots of (a) LP, (b) HP and (c) LP-SB sets of Cu_2O thin-films, consisting of four LP samples, five HP samples and three LP-SB samples deposited using different O_2 flow rates.

With the results observed in the three plots, Table 3.1 summarizes the oxygen flow rate and the bandgaps of the most stoichiometric Cu_2O thin-films.

Table 3.1 – Most stoichiometric Cu_2O thin-films from each set (LP, HP and LP-SB) and respective bandgaps.

	LP	HP	LP-SB
O_2 flow rate (sccm)	1.3	0.8	1.2
Bandgap (eV)	2.57	2.56	2.57

The results obtained by transmittance spectroscopy are in line with the evaluation of the color of the films. In addition, all three samples corresponding to the most stoichiometric Cu_2O thin-films show a consistent bandgap value between 2.56 and 2.57 eV. Although the fundamental bandgap of Cu_2O is 2.17 eV, the estimation using transmittance data generally leads to higher values, since the absorption at lower energy is not resolvable by this technique. [15]

To complete the analysis, a shift to the left between the HP films deposited using 0.8 sccm and 0.7 sccm O₂ flow rates can be observed. The same happens between the LP films deposited using 1.3 sccm and 1.2 sccm O₂ flow rates, although it is not so pronounced.

3.1.2. X-Ray Diffraction

XRD measurements allow investigating the material structure. By comparing the data obtained with references from the International Centre for Diffraction Data (ICDD) database, it is possible to check the presence of a certain material structure. In this case, it was important to verify if phases like CuO, Cu₄O₃ or even metallic copper were present in the films, besides the expected Cu₂O phase. The respective Powder Diffraction File (PDF) numbers of these materials are: Cu₂O (PDF: 00-005-0667); CuO (PDF: 00-045-0937); Cu₄O₃ (PDF: 01-083-1665); Cu (PDF: 00-004-0836).

First, the LP set of films was analyzed. The respective data is represented in Figure 3.2, whereas the database references from the materials mentioned above are represented in Figure 3.3.

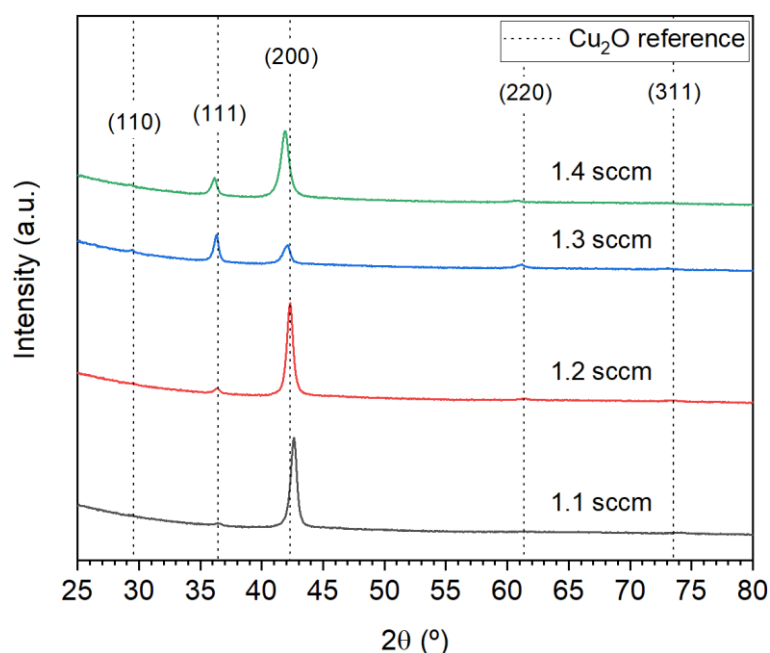


Figure 3.2 – XRD results of the LP set of Cu₂O thin-films, consisting of four samples deposited using different O₂ flow rates. The main peaks of Cu₂O are represented by the dashed lines.

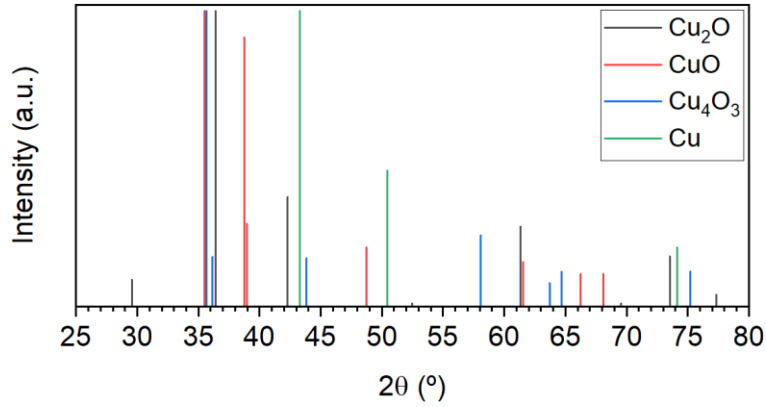


Figure 3.3 – XRD database references of copper oxides (Cu_2O , CuO and Cu_4O_3) and metallic Cu.

Analyzing the diffractograms, it is possible to observe that the main peaks of Cu_2O are present, with no signs of peaks from other materials. This means that all the LP films are formed by Cu_2O , independently of the O_2 flow rate used. Nonetheless, except for the film deposited using a 1.2 sccm O_2 flow rate, the peak position of the films is not the same when compared to the Cu_2O reference. Comparing all the LP films, there is a visible trend when increasing the O_2 flow rate used during the deposition: all the peaks are shifting to the left. Despite not presented here, both LP-SB and HP sets of films show the same behavior (Annex A), which is supported by literature. [16] The mentioned shift can be interpreted by Bragg's law (2), which represents the condition where radiation waves are scattered by a crystalline solid, resulting in a constructive interference phenomenon.

$$2d \sin \theta = n\lambda \quad (2)$$

In the equation, λ represents the wavelength of the incident radiation and θ its glancing angle; d is the distance between consecutive crystallographic planes and n is a positive integer. With Bragg's law in mind, the peak shift to the left (smaller diffraction angles) seen in the films deposited using 1.3 and 1.4 sccm O_2 flow rates can mean the films are under tensile strain (greater distance between crystallographic planes); the peak shift to the right (greater diffraction angles) seen in the film deposited using a 1.1 sccm O_2 flow rate can mean that the film is under compressive strain (smaller distance between crystallographic planes). In summary, an increase of the O_2 flow rate during the deposition process is inducing more tensile strain in the films, possibly due to the inclusion of more copper vacancies in the film. This results in the repulsion of neighboring oxygen anions which consequently leads to a lattice expansion. [17]

As the samples analyzed are thin-films, it is not possible to obtain absolute results on an eventual texturization. The volume illuminated by the X-ray decreases considerably with increasing diffraction angles, leading to a mismatch between the peak heights from the Cu_2O reference and the films themselves. For that reason, only peak position has been analyzed so far. However, most

of the films show a preferential orientation in the (200) direction; the only exception is the most stoichiometric LP film, in which (111) and (200) directions are equally pronounced.

Besides the LP set of films, the most stoichiometric films from each set (LP-SB, LP and HP) were analyzed. The most stoichiometric HP film which was later heated at 100 °C for 24 hours (HP-heated) was also evaluated. It should be noted that the last-mentioned film had gold contacts deposited on it before the XRD measurement, which justifies the Au peaks in its diffractogram. All these results are represented in Figure 3.4.

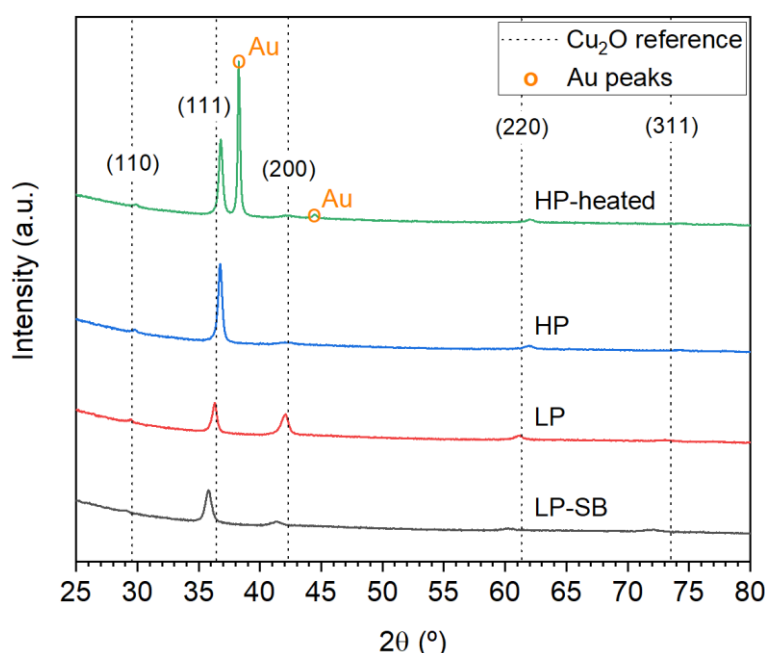


Figure 3.4 – XRD results of the most stoichiometric Cu₂O thin-films from each set (LP-SB, LP and HP), including HP-heated film. The main peaks of Cu₂O are represented by the dashed lines.

As observed, the most stoichiometric films from the LP-SB, LP and HP sets show no signs of peaks from other materials besides Cu₂O. The peak position of either the LP-SB or LP film is shifted to the left, which is more prominent on the first one. This can mean that both these two films are experiencing a tensile strain. On the other side, the HP film has its peaks shifted to the right, which can mean it is experiencing a compressive strain.

The HP-heated film also shows no peaks from other materials besides Cu₂O. Furthermore, the diffractograms of both HP and HP-heated films have the same appearance (besides the obvious Au peaks present on the HP-heated film). This is in line with the desired since the post-deposition heating treatment was supposed to change the properties of the grain boundaries, not the grains.

In spite of the most stoichiometric LP film showing no preferential orientation between (111) and (200) directions, the remaining films from the LP set have the (200) direction more pronounced. On the opposite, the most stoichiometric HP film have a preferential orientation in the

(111) direction, as the majority of the remaining films from the HP set. This shows a trend supported by literature in which a lower deposition pressure promotes the (200) direction as the preferential orientation of the film, whereas a higher deposition pressure promotes the (111) direction. [18]

In a general way, the peaks are relatively broad which means the size of the grains in the film is in the nanometric range.

Below, the diffractograms of two specific films from the HP set are presented in Figure 3.5.

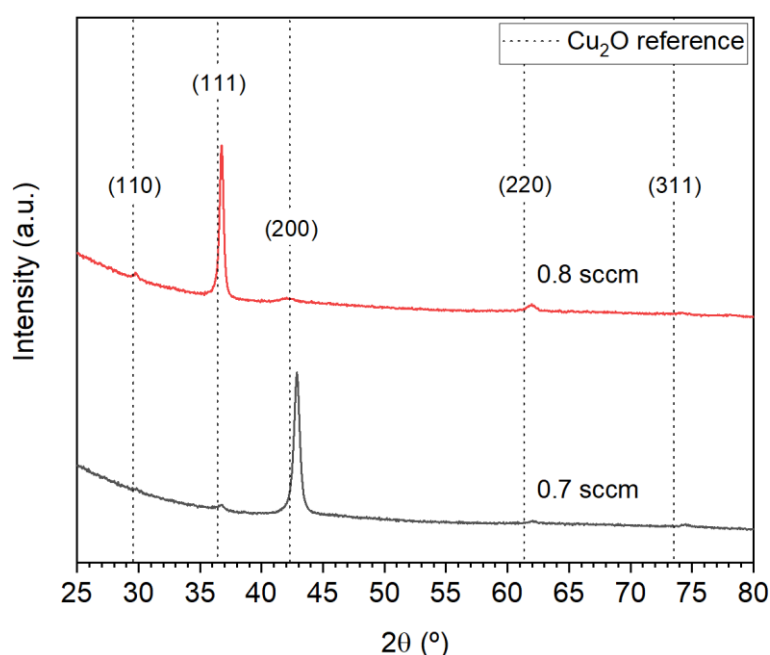


Figure 3.5 – XRD results of two Cu_2O thin-films from the HP set, deposited using 0.7 sccm and 0.8 sccm O_2 flow rates. The main peaks of Cu_2O are represented by the dashed lines.

These two films, although they were deposited using similar O_2 flow rates, have two different preferential orientations. The film deposited using a 0.7 sccm O_2 flow rate has the (200) direction – which is the same as (100) – as preferential orientation, whereas the film deposited using a 0.8 sccm O_2 flow rate is oriented preferentially in the (111) direction. The influence of this property is analyzed in a chapter ahead.

3.1.3. Scanning Electron Microscopy

To complement the information obtained by transmittance spectroscopy and XRD, SEM was used to obtain images that were capable to show the polycrystalline structure of a Cu_2O thin-film. Figure 3.6 displays a cross-section of one of the most stoichiometric Cu_2O films.

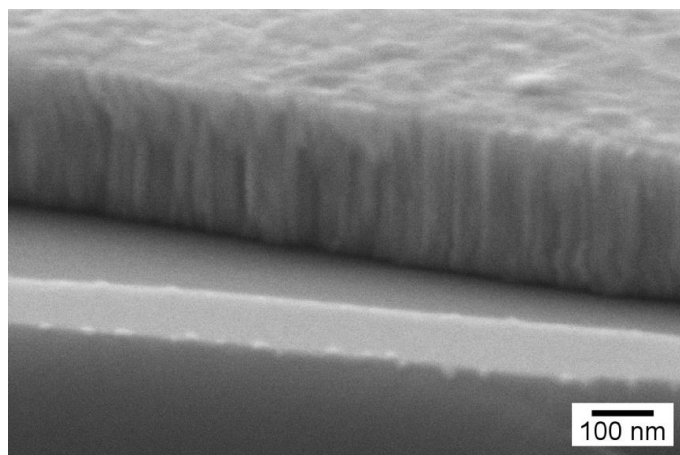


Figure 3.6 – SEM cross-sectional image of the most stoichiometric LP Cu₂O thin-film deposited on a silicon substrate.

First, this SEM image supports the thickness value obtained by profilometry. Considering a 265 nm thickness, the calculated sputtering deposition rate is 4.4 nm/min. In addition, the cross-section of the film shows its polycrystalline structure, namely the columnar shape of the grains.

3.1.4. X-Ray Photoelectron Spectroscopy

XPS was used to understand possible chemical composition differences between the films from the LP set deposited using different O₂ flow rates. Figure 3.7 displays that data, specifically from the most important emissions: Cu 2p and O 1s.

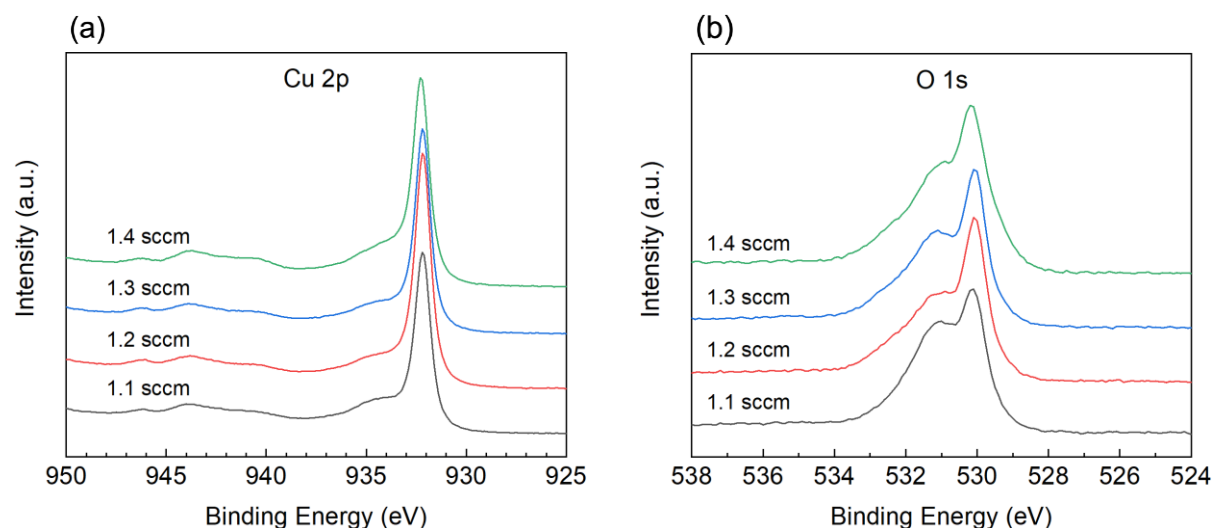


Figure 3.7 – XPS data from (a) Cu 2p and (b) O 1s emissions relative to the LP set of films, consisting of four samples deposited using different O₂ flow rates.

Despite the different O₂ flow rate used in each deposition, the results obtained are very similar among all the LP films, showing between 55% and 60% of oxygen, which indicates a strong CuO presence. It is worth referring that XPS is a technique that is only sensitive to the first 5-10 nm

from the surface. For that reason, these results were already expected since Cu₂O films oxidize easily while exposed to air and the XPS measurements were performed *ex situ* [2].

3.1.5. Atomic Force Microscopy and Conductivity Measurements

The last technique used to analyze the Cu₂O thin-films was AFM/CAFM. These techniques allow obtaining information about the topography and local conductivity of a material in a very detailed way, which is useful due to the polycrystalline structure of these films. For a complementary reason, conductivity measurements made by the van der Pauw method are also presented in this chapter.

Among the different films, the average grain current (I_G) was the factor that changed the most. To analyze that, *Gwyddion*'s potentialities were used. First, the current values were corrected by replacing the data that did not satisfy the 3σ criteria. Then, a mask that covers the less conductive part of the film (the grain boundaries) is applied. That mask contains the points with the 20% lower current values from the scale. Finally, the average current is calculated on the areas outside the mask (grains). In Figure 3.8 there is an example of the process used for all the films. The mask is represented in red.

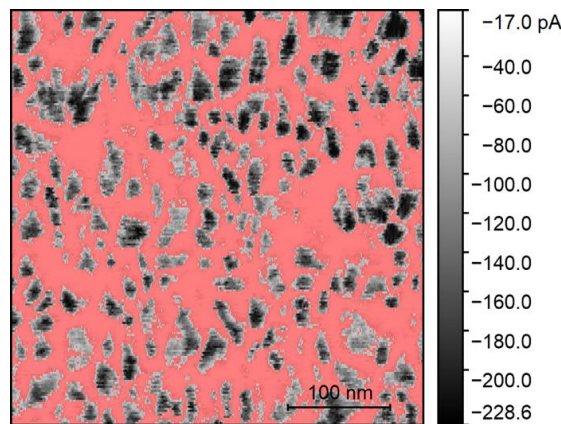


Figure 3.8 – Mask applied by *Gwyddion* software. The I_G was measured outside the mask.

Whereas the van der Pauw method can provide information about in-plane conductivity of the films (σ_{IP}), CAFM is able to provide information about out-of-plane conductivity of the grains (σ_{OOP-G}), which is calculated by Equation 3.

$$\sigma_{OOP-G} = \frac{I_G}{V_{CAFM}} \cdot \frac{t_{film}}{A_{tip}} \quad (3)$$

In this formula, I_G represents the average grain current obtained by the method explained above, V_{CAFM} is the voltage used during CAFM measurements (2 V) and t_{film} represents the thickness of the film. In addition, the AFM tip was considered a sphere with a 25 nm radius. A_{tip} is the area of its bigger cross-section.

First, the LP set of films was analyzed. In Figure 3.9 it is possible to observe both topographic images and current maps of those films.

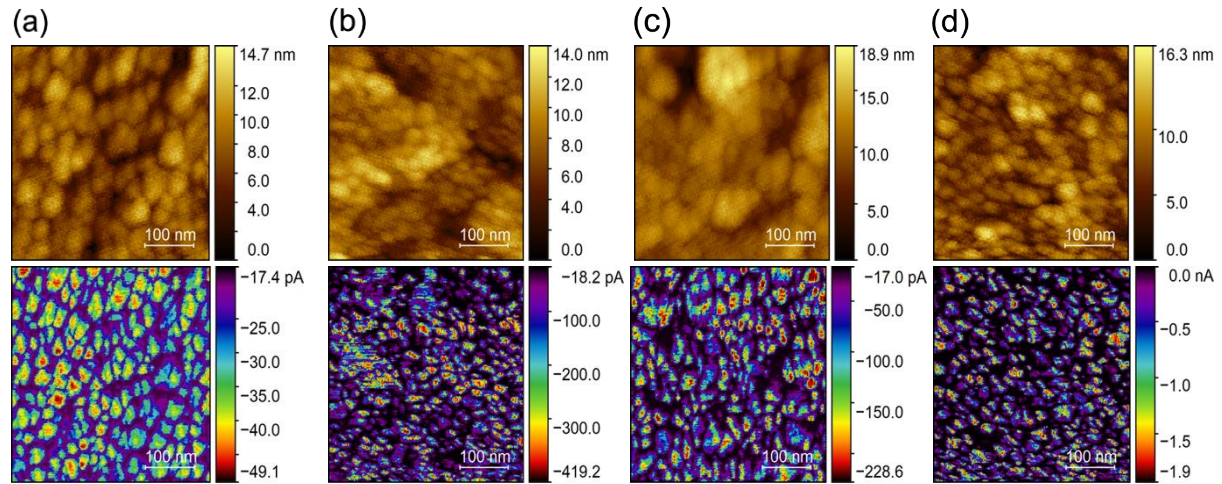


Figure 3.9 – Topographic images and respective current maps of every Cu_2O thin-film from the LP set, consisting of four samples deposited using different O_2 flow rates: (a) 1.1 sccm, (b) 1.2 sccm, (c) 1.3 sccm and (d) 1.4 sccm.

As observed in the topographic images, the polycrystalline structure of the films is immediately visible. The grains have dimensions in the order of dozens of nanometers (supported by XRD and SEM) and the film roughness varies between 14 and 19 nm.

Regarding the current maps, it is important to refer that the range of currents measured is negative due to the voltage polarity used (-2 V). From now on, only absolute values will be referred. In these images, the polycrystalline structure of the films becomes more evident and there is an obvious difference in the conduction properties when comparing the grains and the grain boundaries. Conduction happens mostly inside the grains, whereas the grain boundaries have a negligible amount of current passing through. As observed, the lowest current value measured is very similar through all the films (around -17 pA), which leads to the conclusion that it could be a current offset of the equipment. Although the oxygen flow rate used during deposition does not change the fact that the grains are more conductive than the grain boundaries, it has an evident influence on the range of current values measured on the grains.

In Table 3.2, in-plane and out-of-plane conductivities of every LP film are compared.

Table 3.2 – I_G , σ_{OOP-G} and σ_{IP} of every Cu_2O thin-film from the LP set, consisting of four samples deposited using different O_2 flow rates.

LP set: O_2 flow rate (sccm)	1.1	1.2	1.3	1.4
I_G (pA)	33	215	126	925
σ_{OOP-G} ($\mu S/cm$)	22.3	145.1	85.0	624.2
σ_{IP} (mS/cm)	1.8	-	3.1	8.1

There is a general trend in which the σ_{OOP-G} seems to get higher as the oxygen flow rate used during the deposition of the film is higher. The film deposited using the lowest oxygen flow rate has the lowest σ_{OOP-G} (22.3 $\mu S/cm$), whereas the film deposited using the highest oxygen flow rate has the highest σ_{OOP-G} (624.2 $\mu S/cm$), more than one order of magnitude above. For that reason, it is possible to conclude that more oxidized films have greater σ_{OOP-G} . The film deposited using a 1.3 sccm oxygen flow rate (the most stoichiometric one among LP films) is the only one that deviates from this trend, having a lower σ_{OOP-G} (85.0 $\mu S/cm$). This can be due to differences on its preferential orientation compared to the other LP films (Figure 3.2).

In terms of σ_{IP} , one of the films could not be measured, though there seems to be a similar trend: σ_{IP} is also higher when the films are deposited using a higher O_2 flow rate.

After comparing all the LP films, the most stoichiometric films deposited under the three different main conditions were compared. The most stoichiometric HP film which was later heated was also analyzed. The corresponding topographic images and current maps are displayed in Figure 3.10.

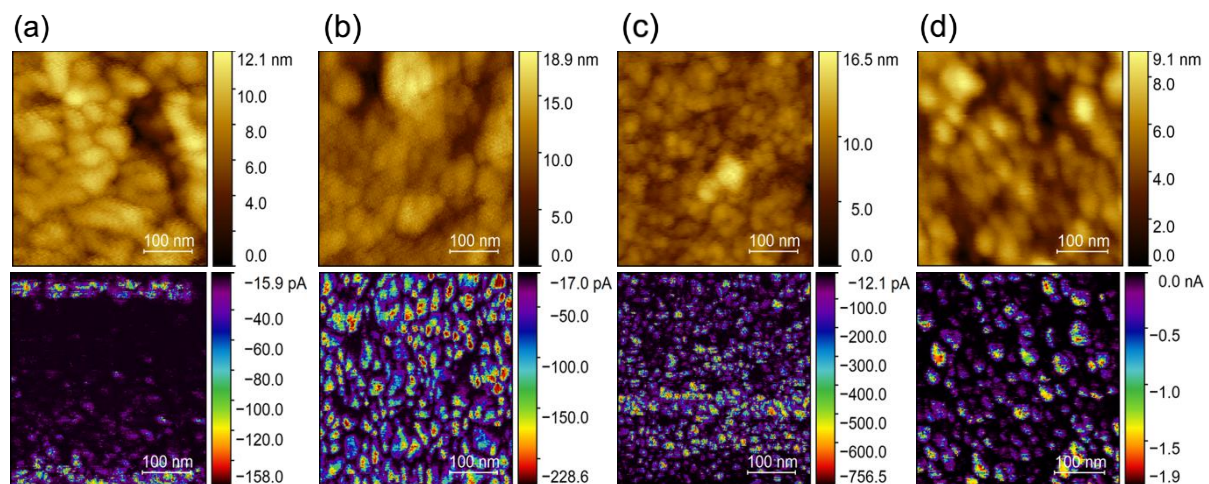


Figure 3.10 – Topographic images and respective current maps of the most stoichiometric Cu_2O thin-films from each set: (a) LP-SB, (b) LP and (c) HP, including (d) HP-heated film.

Comparing these results with the previous ones, there are no apparent differences regarding the fact that grains are still more conductive than the grain boundaries. This leads to the conclusion

that this behavior does not get altered by using different chamber pressures, by applying a substrate bias, or even by heating the films. Nonetheless, average current values measured on the grains keep changing. Those values are presented in Table 3.3 in conjunction with out-of-plane and in-plane conductivities.

Table 3.3 – I_G , σ_{OOP-G} and σ_{IP} of the most stoichiometric Cu_2O thin-films from each set, including HP-heated film.

Most stoichiometric films: deposition conditions	LP-SB	LP	HP	HP-heated
I_G (pA)	78	126	344	880
σ_{OOP-G} ($\mu S/cm$)	52.6	85.0	232.1	593.8
σ_{IP} (mS/cm)	2.0	3.1	0.8	4.0

Comparing the most stoichiometric films from each set (LP-SB, LP, HP), it is possible to verify that σ_{OOP-G} increases in this order: LP-SB; LP; HP. Considering the same order, XRD measurements showed that the films are experiencing an increased compressing strain (Figure 3.4). Since these films are all stoichiometric, copper vacancies cannot be the cause of the lattice expansion. This leads to the conclusion that the improved conductivity can be related to the more compressed structure of the films, which may be associated with a higher densification state.

Relatively to the post-deposition heating treatment, it seems to increase the grain conductivity since the HP-heated film has a σ_{OOP-G} significantly higher than the HP film. A heating treatment oxidizes the films, similarly to what an increase of the O_2 flow rate does. That is in line with the previous results in which more oxidized films had more conductive grains (Table 3.2).

In terms of σ_{IP} , it seems to follow the same trend as σ_{OOP-G} , except for the most stoichiometric HP film, which has the lowest value among the analyzed films.

After observing that deposition conditions such as pressure, oxygen flow rate, substrate bias or even a post-deposition heating treatment do not influence the more-conductive-grain behavior, shorter depositions were made while keeping other factors constant. That way it was possible to understand if the thickness of the film had any influence on this behavior. In this case, the conditions used to obtain the most stoichiometric LP film were used. The respective topographic images and current maps are displayed in Figure 3.11.

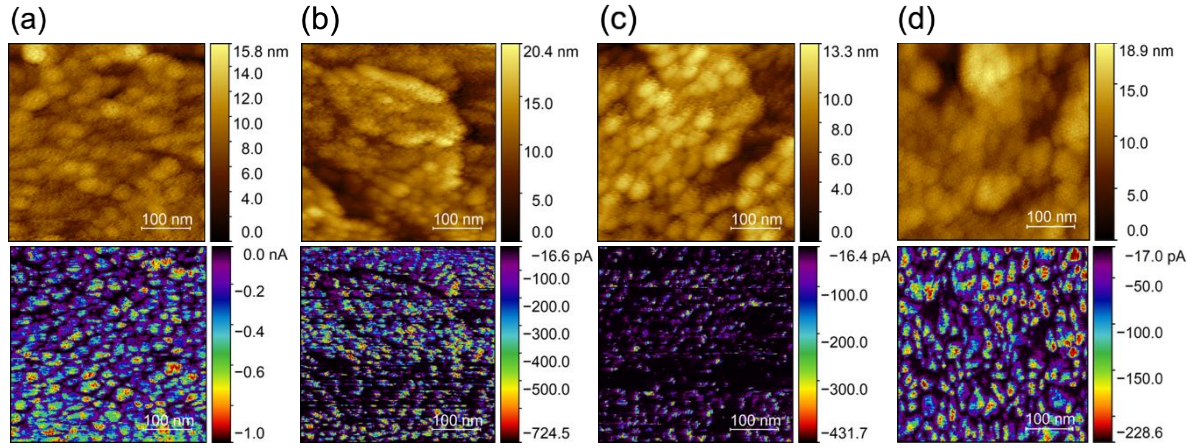


Figure 3.11 – Topographic images and respective current maps of Cu_2O thin-films deposited under the same conditions as the most stoichiometric film from the LP set, consisting of four samples deposited during different times: (a) 7.5 minutes, (b) 15 minutes, (c) 30 minutes and (d) 60 minutes.

Once more, the thickness of the films does not change the fact that the grains are more conductive than the grain boundaries. The average current values measured on the grains, as also out-of-plane and in-plane conductivities are shown in Table 3.4.

Table 3.4 – I_G , $\sigma_{\text{OOP-G}}$ and σ_{IP} of Cu_2O thin-films deposited under the conditions of the most stoichiometric film from the LP set, consisting of four samples deposited during different times.

Most stoichiometric - LP set: deposition time (min)	7.5	15	30	60
I_G (pA)	438	324	198	126
$\sigma_{\text{OOP-G}}$ ($\mu\text{S/cm}$)	37.0	54.7	66.8	85.0
σ_{IP} (mS/cm)	13.8	7.8	4.1	3.1

As verified, the increase of the film thickness slightly increases $\sigma_{\text{OOP-G}}$. On the opposite, σ_{IP} decreases when the film thickness increases.

To understand the possible influence of the preferential orientation of the films on their electrical properties, the same two HP films discussed in the XRD chapter are analyzed here. Their respective topographic images and current maps are presented in Figure 3.12.

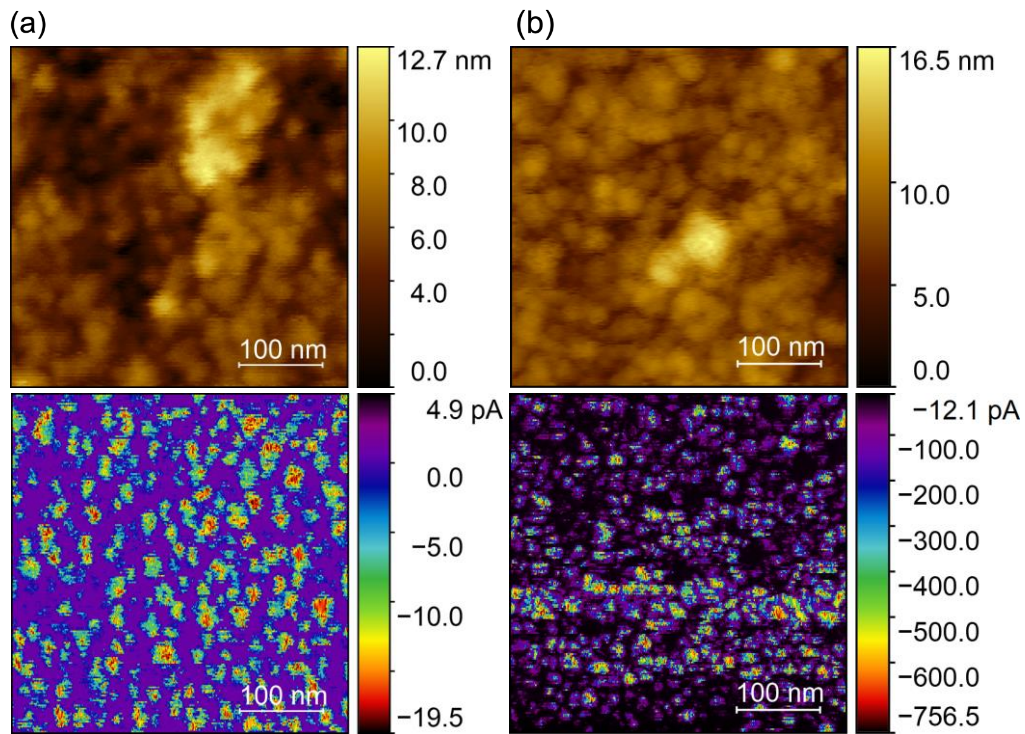


Figure 3.12 – Topographic images and respective current maps of Cu₂O thin-films from the HP set with different preferential orientations, consisting of two samples deposited using different O₂ flow rates: (a) 0.7 sccm and (b) 0.8 sccm.

Once again, the grains are still more conductive than the grain boundaries. Information relative to the average current measured on the grains and out-of-plane and in-plane conductivities are summarized in Table 3.5. Besides these results, resistivity measurements performed on the complete HP set of films, including data related to post-deposition heating treatments of different durations, are included in Annex B.

Table 3.5 – I_G , σ_{OOP-G} and σ_{IP} of Cu₂O thin-films from the HP set with different preferential orientations, consisting of two samples deposited using different O₂ flow rates.

HP set: O ₂ flow rate (sccm)	0.7	0.8
Preferential Orientation	(200) = (100)	(111)
I_G (pA)	15	344
σ_{OOP-G} ($\mu S/cm$)	10.1	232.1
σ_{IP} (mS/cm)	86.8	840.4

Analyzing these results, σ_{OOP-G} seems to be considerably higher on the (111)-oriented film than on the film oriented in the (100) direction, which is supported by literature. [11] Having in mind the columnar structure of the Cu₂O thin-films observed by the cross-sectional SEM images (Figure 3.6), the interface between grains should have the same orientation as the surface. This assumption seems correct since σ_{IP} shows the same tendency as σ_{OOP-G} .

Previously, emphasize was put on metallic particle formation and associated depletion of Cu_2O to explain these differences in electrical conductivity. [7] However, the above indicates a strong contribution of the grain orientation to the current transport over its interfaces. The main conclusion is that (111) preferential orientation seems to promote a better charge carrier transport, compared to (100) direction.

Indeed, previous works showed that Cu_2O thin-films that were (111)-oriented had increased grain boundary conductivity. [4], [8] The (111) interface also has a higher tendency to oxidize. [9]

To better investigate the influence of the preferential orientation of the films, Kelvin probe force microscopy (KPFM) measurements were performed. [19] However, the images do not lead to any conclusion due to the small size of the grains compared to the resolution allowed by the equipment. Those results are present in Annex C.

All the images above were obtained by applying a -2 V voltage to the films. Different voltage values were tested, as also different polarities. In Figure 3.13 there is an example of an image obtained by changing the voltage polarity in the middle of the process.

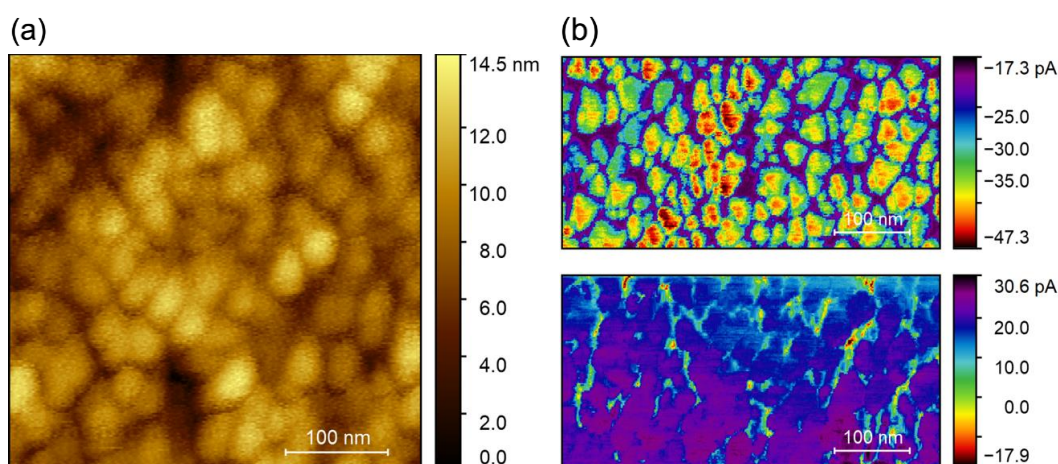


Figure 3.13 – (a) Topographic image and (b) respective current map of the LP film deposited using a 1.1 sccm O_2 flow rate. The top half of either image was obtained by using a -2 V voltage and the bottom half using a +2 V voltage.

There are no visible differences regarding the topographic image. One advantage of using a -2V voltage compared to a +2 V voltage is the better contrast obtained in the current map between the grains and the grain boundaries. Although, that does not change the behavior of grains being more conductive compared to the grain boundaries.

A different AFM equipment was also tested to verify if it would show different results. Both the topographic image and the current map of one of the most stoichiometric films are presented in Figure 3.14.

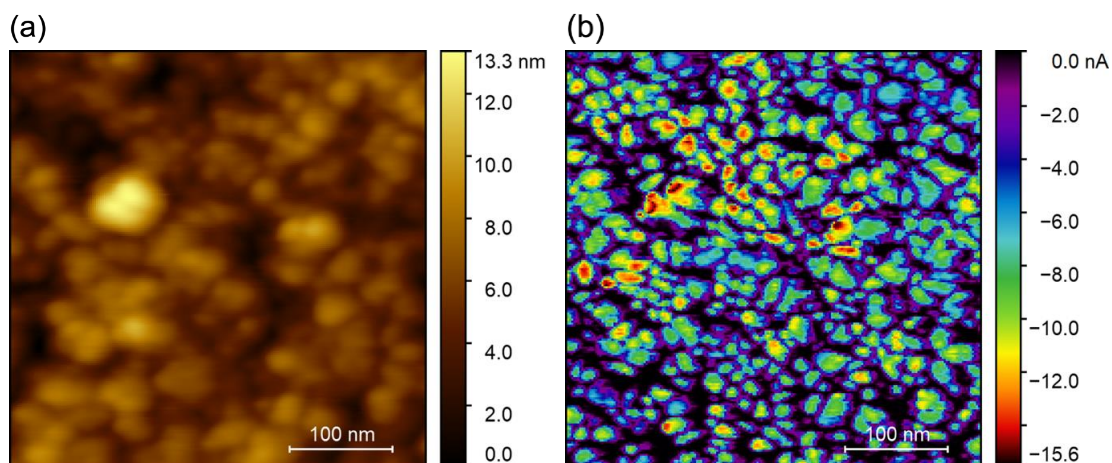


Figure 3.14 – (a) Topographic image and (b) respective current map of the most stoichiometric Cu_2O thin-film from the HP set obtained by *Cypher S*.

The images above are visibly clearer and more stable than the images of the same film made with the *MFP-3D-SA* system (Figure 3.10 (c)). Both images show no drift and the contrast between the grains and the grain boundaries is significantly better, mainly in the current map. However, the grains are still more conductive than the grain boundaries, which allows concluding that the equipment has no influence on this behavior.

3.2. Particles

3.2.1. Scanning Electron Microscopy

The shape of the particles was the most important property to be assured, so SEM was the first technique used. The process was optimized, and the particles were grown into the desired shapes. Figure 3.15 shows the results obtained in one synthesis (1st synthesis) and Figure 3.16 shows the results obtained in a posterior synthesis (2nd synthesis).

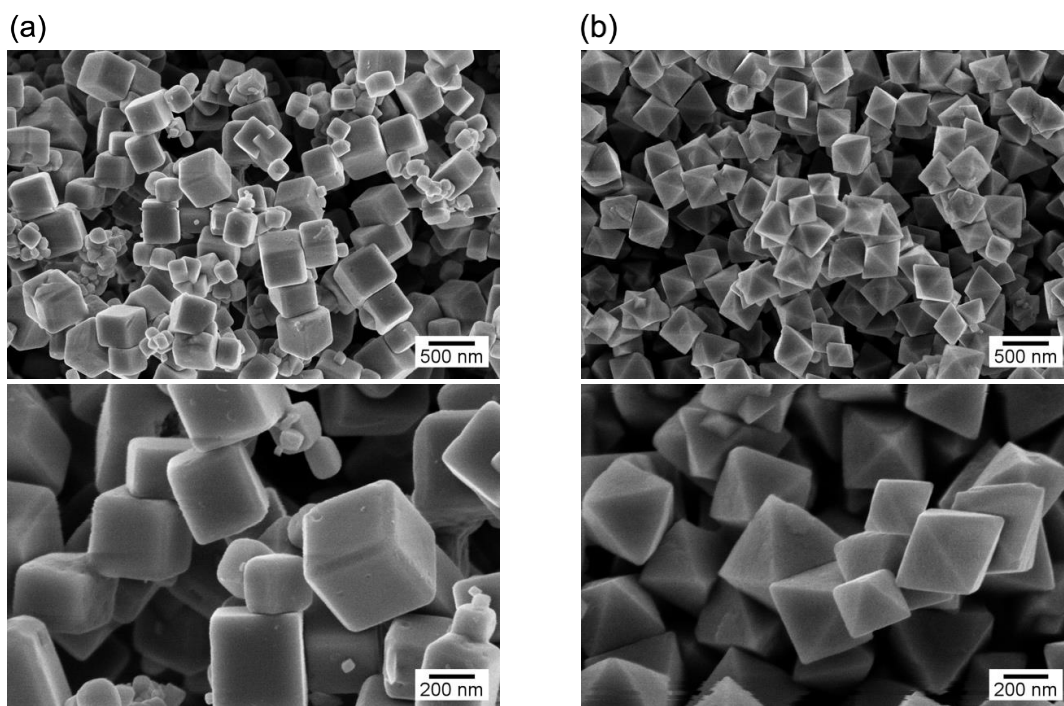


Figure 3.15 – SEM images of (a) cubic and (b) octahedral particles obtained in the 1st synthesis.

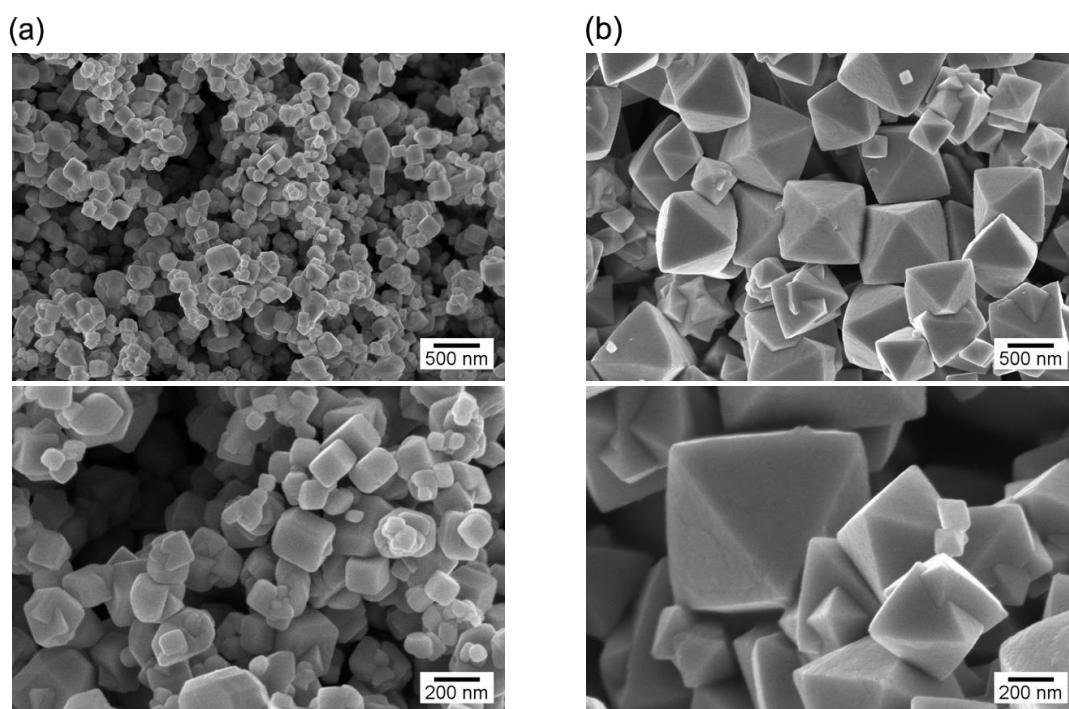


Figure 3.16 – SEM images of (a) cubic and (b) octahedral particles obtained in the 2nd synthesis.

In the 1st synthesis, particles of either shape had a similar size, around 400 nm. Although, cubic particles showed a greater size dispersion compared to the octahedral ones. In the 2nd synthesis, the shape of both cubic and octahedral particles was not so perfect as before. Both showed a considerable size dispersion and the presence of agglomerates. Besides that, cubic particles became smaller (around 200 nm) and octahedral particles became bigger (around 700 nm) when compared to the 1st synthesis.

3.2.2. X-Ray Diffraction

To identify other possible phases besides Cu_2O that could be present in the particles, XRD measurements were performed. The diffractograms relative to the particles obtained in the 1st synthesis are shown in Figure 3.17.

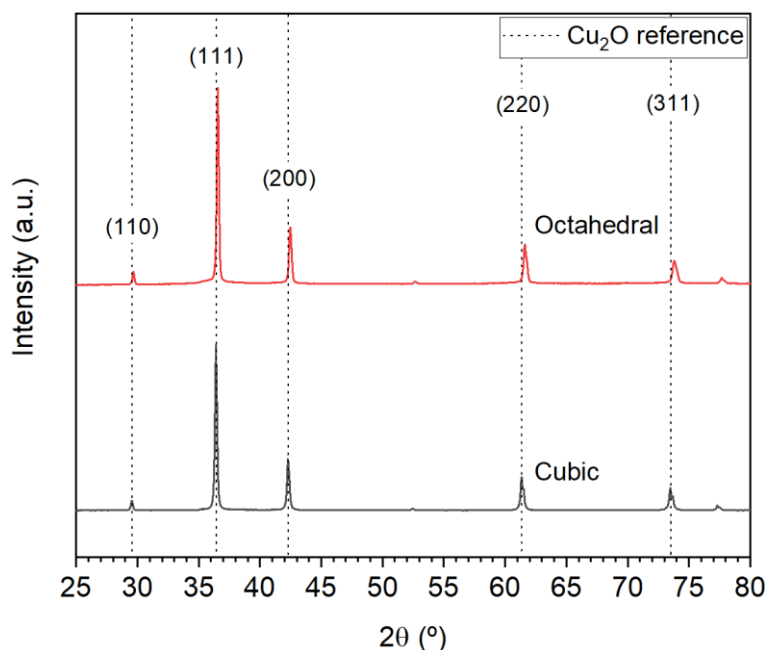


Figure 3.17 – XRD results from cubic and octahedral particles obtained in the 1st synthesis. The main peaks of Cu_2O are represented by the dashed lines.

Diffractograms from both shapes of particles are identical and represent an almost-perfect match with the Cu_2O pattern. Only the octahedral particles show a slight peak shift to the right, which can suggest the structure is under a compressive strain. In terms of peak height, both particles fit the pattern precisely. Observing the width of the peaks, the immediate conclusion is that the crystallite size must be bigger than what is observed in the films (Figure 3.4). Probably, each particle consists on a single crystalline domain.

3.2.3. Energy Dispersive X-Ray Spectroscopy

EDS allows obtaining information about the chemical composition of the particles. Cubic and octahedral particles from both syntheses were analyzed and the results are displayed in Table 3.6.

Table 3.6 – Oxygen content of cubic and octahedral particles from both syntheses, obtained by EDS.

Oxygen content (%)	1 st synthesis	2 nd synthesis
Cubic	16.6	29.4
Octahedral	30.2	24.0

The EDS results obtained from the particles, although not showing a 2:1 Cu/O proportion, all suggest a stronger presence of copper compared to oxygen, with a signal at least twice more intense. Independently of the particle shape, the smaller particles (cubic – 2nd; octahedral – 1st), which have a superior surface/body ratio, show a stronger oxygen presence than the bigger ones (respectively: cubic – 1st; octahedral – 2nd), which leads to the conclusion that possibly the surface of the particles is more oxidized than their inside. XPS measurements were also performed, nonetheless, they did not provide any consistent conclusion. Those results are present in Annex D.

3.2.4. Atomic Force Microscopy

To understand the influence of the facets on the conductive properties of Cu₂O, several AFM/CAFM measurements were performed on particles of both shapes.

The synthesis was still unoptimized when the first images were tested. A topographic image and a current map of unoptimized octahedral particles can be observed in Figure 3.18. The system used was a *Cypher S* and the current map was obtained with no voltage applied to the substrate.

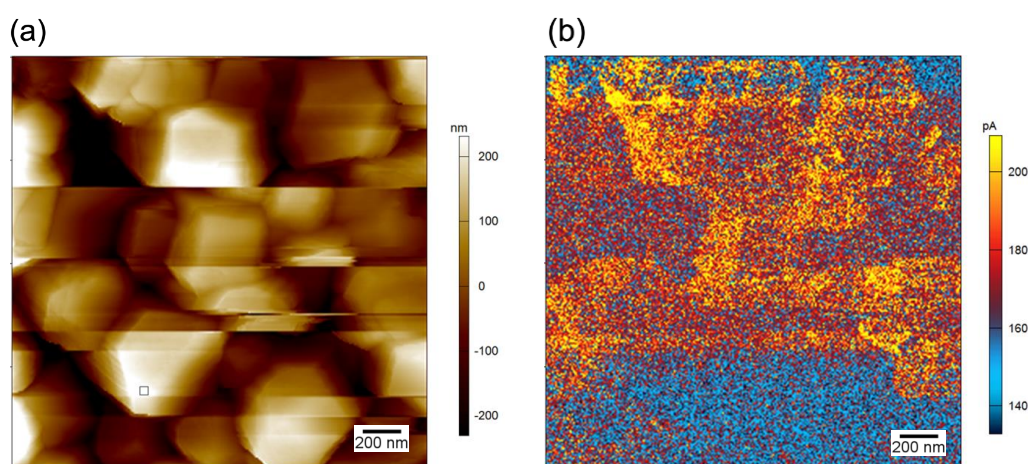


Figure 3.18 – (a) Topographic image and (b) respective current map of unoptimized octahedral particles obtained by a *Cypher S* system.

After optimizing the synthesis, *MFP-3D-SA* system was used to obtain similar images of the octahedral particles from the 1st synthesis. The process to obtain images with good resolution took dozens of hours which promoted some issues related to drift and loss of contact with the surface. For that reason, only the low-resolution images present in Figure 3.19 could be obtained.

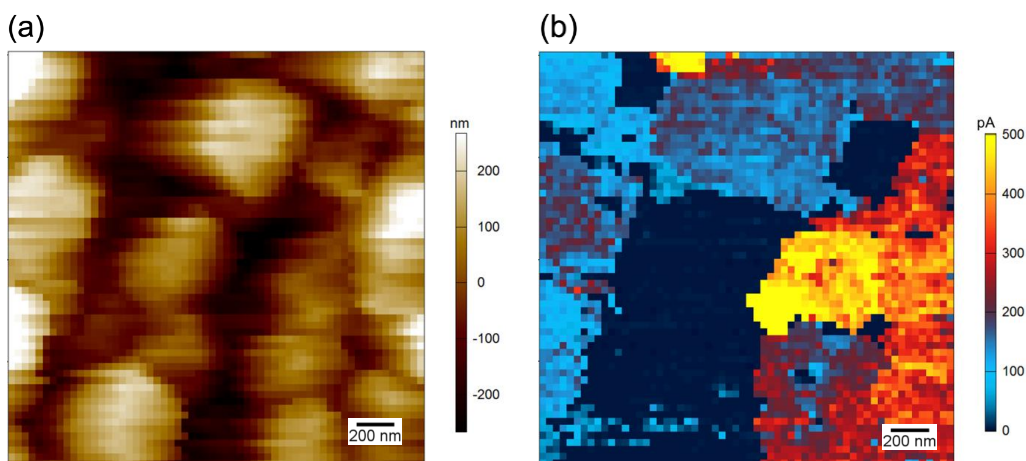


Figure 3.19 – (a) Topographic image and (b) respective current map of octahedral particles from the 1st synthesis obtained by a *MFP-3D-SA* system.

Posteriorly, it was possible to analyze the same particles with a different equipment, a *Nano-Observer* system. The respective topographic images and resistivity maps are shown in Figure 3.20.

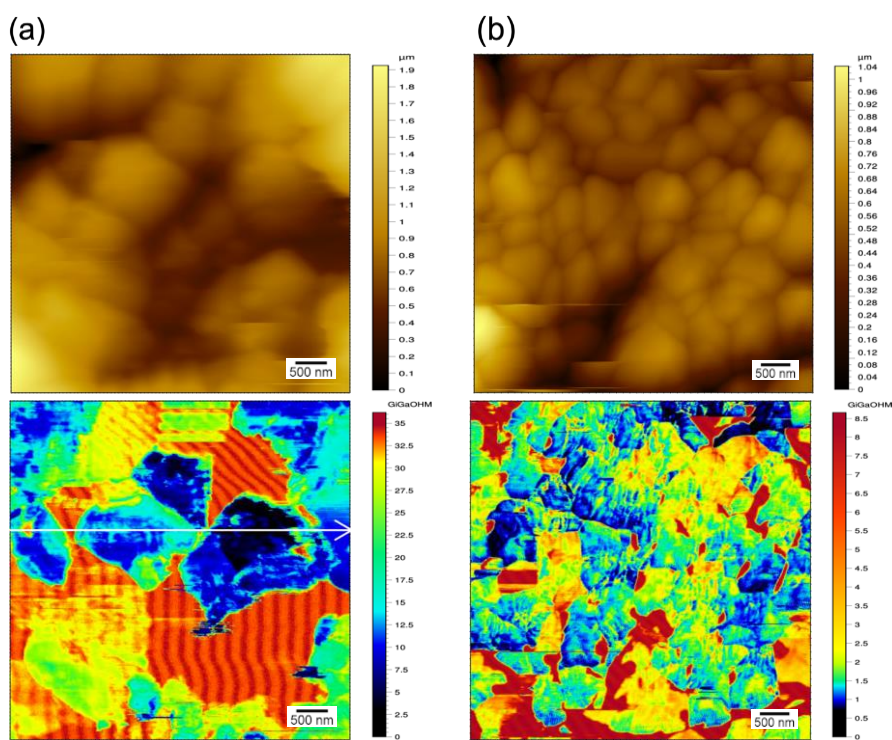


Figure 3.20 – Topographic images and respective resistivity maps of (a) cubic and (b) octahedral particles from the 1st synthesis. Images obtained by a *Nano-Observer* system.

Images from Figure 3.18 and Figure 3.19 do not have enough quality that allows taking any conclusion. Figure 3.20, despite not showing the exact shape of the particles on the topographic images, seems to show some differences in the resistivity. Cubic particles seem to be more resistive than the octahedral ones, which is in line with the literature. [11]

4. Conclusions and Future Perspectives

In this work, Cu_2O thin-films were successfully produced by reactive sputter deposition. After altering several conditions, such as deposition pressure, oxygen flow rate, substrate bias, deposition time and post-deposition heating treatment, films with more conductive grain boundaries could not get achieved. Instead, Cu_2O films with more conductive grains were obtained.

Transmittance spectroscopy allowed measuring the bandgap of the most stoichiometric Cu_2O films. The value obtained was 2.57 eV, higher than the 2.17 eV referenced, nonetheless, it was expected due to limitations of this technique.

XRD measurements showed that the films experience more tensile strain as their oxygen content increases due to the presence of copper vacancies. Besides that, XRD shows that different deposition pressures and the substrate bias modify the crystallographic lattice, possibly related to differences in the densification state of the films.

SEM revealed the columnar growth of the grains inside the film, whereas XPS confirmed the easy oxidation of the Cu_2O thin-films when exposed to air.

AFM/CAFM, in conjunction with conductivity measurements, showed that the films with greater oxygen content are more conductive; when comparing films with the same oxygen content, it seems that the more compressed films are more conductive. A post-deposition heating treatment oxidizes the films, which increases their conductivity. Curiously, two films deposited under the same conditions with similar oxygen contents showed very different electrical properties. This is thought to be related to the preferential orientation of the films: the film preferentially oriented in the (111) direction is significantly more conductive than the (100)-oriented.

Besides the films, particles of cubic and octahedral shapes were successfully produced from solution. XRD showed that the particles were made from Cu_2O , and EDS, although not providing an exact Cu/O ratio of 2:1, supported those results.

AFM/CAFM measurements on the particles proved to be extremely difficult to perform. Despite the different approaches that were made to prepare the particles and the different systems tested, the steep topography of the samples was a constant issue. However, one of the measurements seems to indicate that octahedral particles – (111) facets – are more conductive than cubic ones – (100) facets.

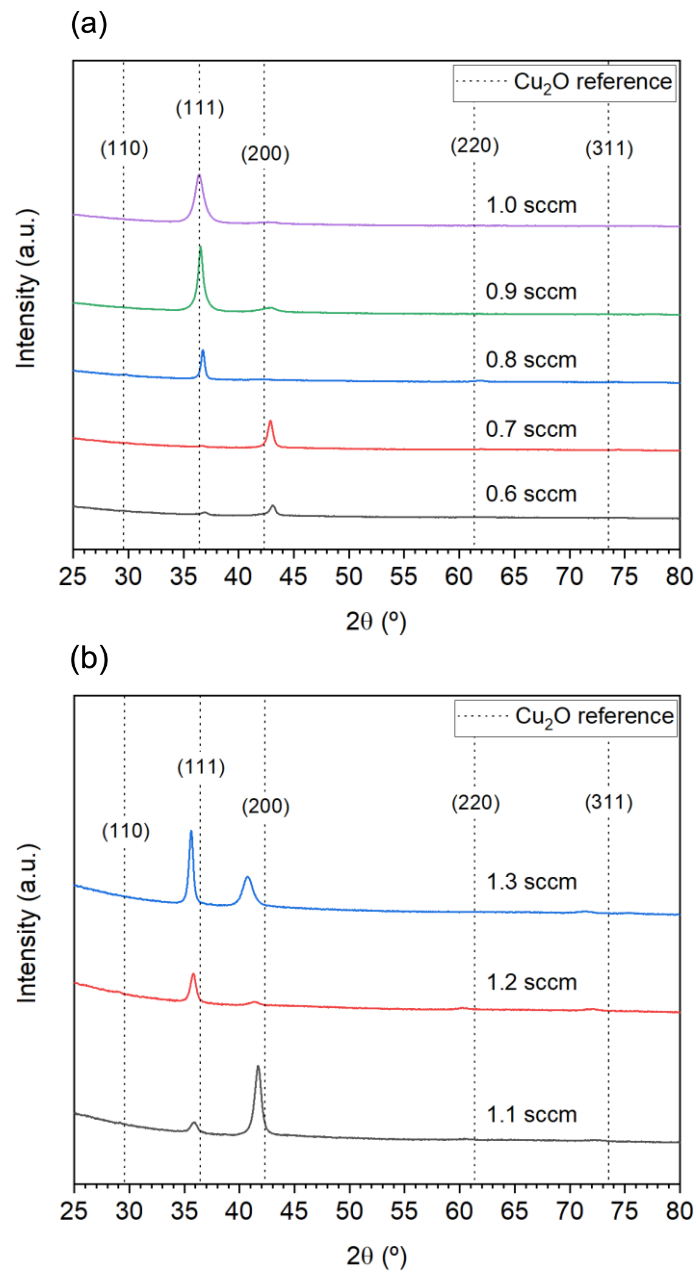
To conclude, preferential orientation of grain interfaces in a film seems to be a factor with some importance on the electrical properties of the film. Undoubtedly, XRD is a good technique to be used when producing thin-films.

References

- [1] H. A. Al-Jawhari, "A review of recent advances in transparent p-type Cu₂O-based thin film transistors," *Mater. Sci. Semicond. Process.*, vol. 40, pp. 241–252, 2015.
- [2] J. Deuermeier *et al.*, "Highly conductive grain boundaries in copper oxide thin films," *J. Appl. Phys.*, vol. 119, no. 23, 2016.
- [3] Y. S. Lee, M. T. Winkler, S. C. Siah, R. Brandt, and T. Buonassisi, "Hall mobility of cuprous oxide thin films deposited by reactive direct-current magnetron sputtering," *Appl. Phys. Lett.*, vol. 98, no. 19, p. 192115, 2011.
- [4] J. Deuermeier *et al.*, "Visualization of nanocrystalline CuO in the grain boundaries of Cu₂O thin films and effect on band bending and film resistivity," *APL Mater.*, vol. 6, p. 096103, 2018.
- [5] C. Das *et al.*, "Effect of Grain Boundary Cross-Section on the Performance of Electrodeposited Cu₂O Photocathodes," *J. Phys. Chem. C*, vol. 122, no. 3, pp. 1466–1476, 2018.
- [6] J. Deuermeier, H. Liu, L. Rapenne, R. Martins, and D. Mu, "Visualization of nanocrystalline CuO in the grain boundaries of Cu₂O thin films and effect on band bending and film resistivity," *APL Mater.*, vol. 096103, 2018.
- [7] S. Siol *et al.*, "Band Alignment Engineering at Cu₂O/ZnO Heterointerfaces," *ACS Appl. Mater. Interfaces*, vol. 8, no. 33, pp. 21824–21831, Aug. 2016.
- [8] H. Liu *et al.*, "The Role of Humidity in Tuning the Texture and Electrical Properties of Cu₂O Thin Films Deposited via Aerosol-Assisted CVD," *Adv. Mater. Interfaces*, vol. 6, no. 3, pp. 1–10, 2019.
- [9] Y. Su, H. Li, H. Ma, J. Robertson, and A. Nathan, "Controlling Surface Termination and Facet Orientation in Cu₂O Nanoparticles for High Photocatalytic Activity: A Combined Experimental and Density Functional Theory Study," *ACS Appl. Mater. Interfaces*, vol. 9, no. 9, pp. 8100–8106, 2017.
- [10] Y. B. Vogel, J. Zhang, N. Darwish, and S. Ciampi, "Switching of current rectification ratios within a single nanocrystal by facet-resolved electrical wiring," *ACS Nano*, vol. 12, no. 8, pp. 8071–8080, 2018.
- [11] C. S. Tan, S. C. Hsu, W. H. Ke, L. J. Chen, and M. H. Huang, "Facet-dependent electrical conductivity properties of Cu₂O crystals," *Nano Lett.*, vol. 15, no. 3, pp. 2155–2160, 2015.
- [12] C. H. Kuo and M. H. Huang, "Facile synthesis of Cu₂O nanocrystals with systematic shape evolution from cubic to octahedral structures," *J. Phys. Chem. C*, vol. 112, no. 47, pp. 18355–18360, 2008.
- [13] D. F. Zhang, H. Zhang, L. Guo, K. Zheng, X. D. Han, and Z. Zhang, "Delicate control of crystallographic facet-oriented Cu₂O nanocrystals and the correlated adsorption ability," *J. Mater. Chem.*, vol. 19, no. 29, pp. 5220–5225, 2009.
- [14] J. Deuermeier, "Origins of limited electrical performance of polycrystalline Cu₂O thin-film transistors" (Doctoral dissertation). Universidade Nova de Lisboa, Portugal; Technische Universität Darmstadt, Germany. 2016.
- [15] B. K. Meyer *et al.*, "Binary copper oxide semiconductors: From materials towards devices," *Phys. Status Solidi B*, vol. 249, no. 8, pp. 1487–1509, Aug. 2012.
- [16] H. Zhu, J. Zhang, X. Lan, C. Li, T. Wang, and B. Huang, "Photo-catalytic activity of Cu₂O films with various crystal structures prepared by DC reactive magnetron sputtering," *Mater. Sci. Forum*, vol. 610–613, pp. 293–298, 2009.
- [17] J. Deuermeier, J. Gassmann, J. Brötz, and A. Klein, "Reactive magnetron sputtering of Cu₂O: Dependence on oxygen pressure and interface formation with indium tin oxide," *J. Appl. Phys.*, vol. 109, no. 11, p. 113704, 2011.
- [18] Y. Wang, "Controllable growth, microstructure and electronic structure of copper oxide thin films" (Doctoral dissertation). Université de Lorraine, France. 2018.
- [19] N. Nicoara *et al.*, "Direct evidence for grain boundary passivation in Cu(In,Ga)Se₂ solar cells through alkali-fluoride post-deposition treatments," *Nat. Commun.*, vol. 10, no. 1, pp. 1–8, 2019.

Annexes

Annex A



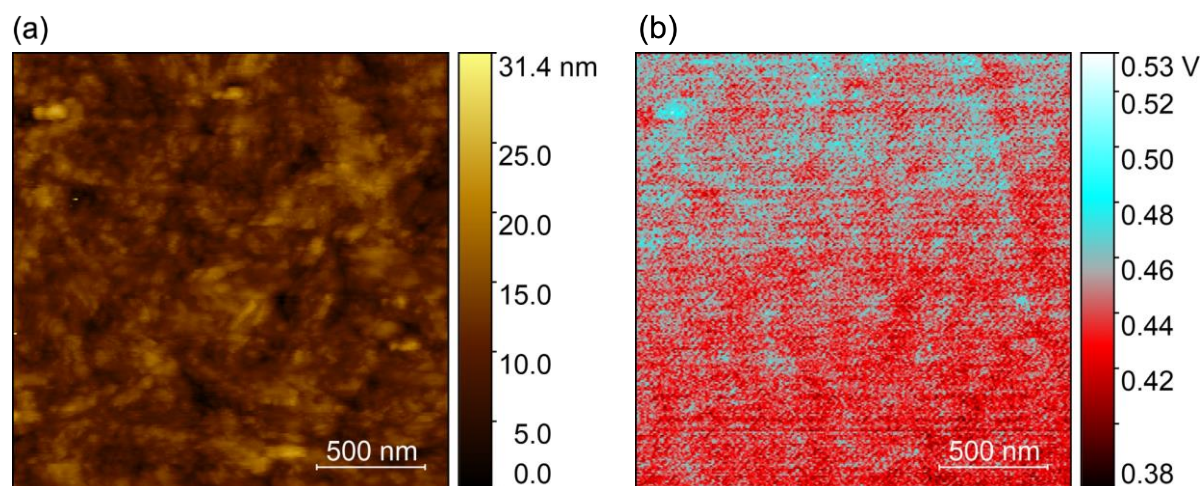
XRD results of every film from: (a) HP set, consisting of five samples deposited using different O_2 flow rates; (b) LP-SB set, consisting of three samples deposited using different O_2 flow rates. The main peaks of Cu_2O are represented by the dashed lines.

Annex B

Resistivity values ($\Omega \text{ cm}$) measured by the van der Pauw method of every film from the HP set. Influence of post-deposition heating treatment of different durations.

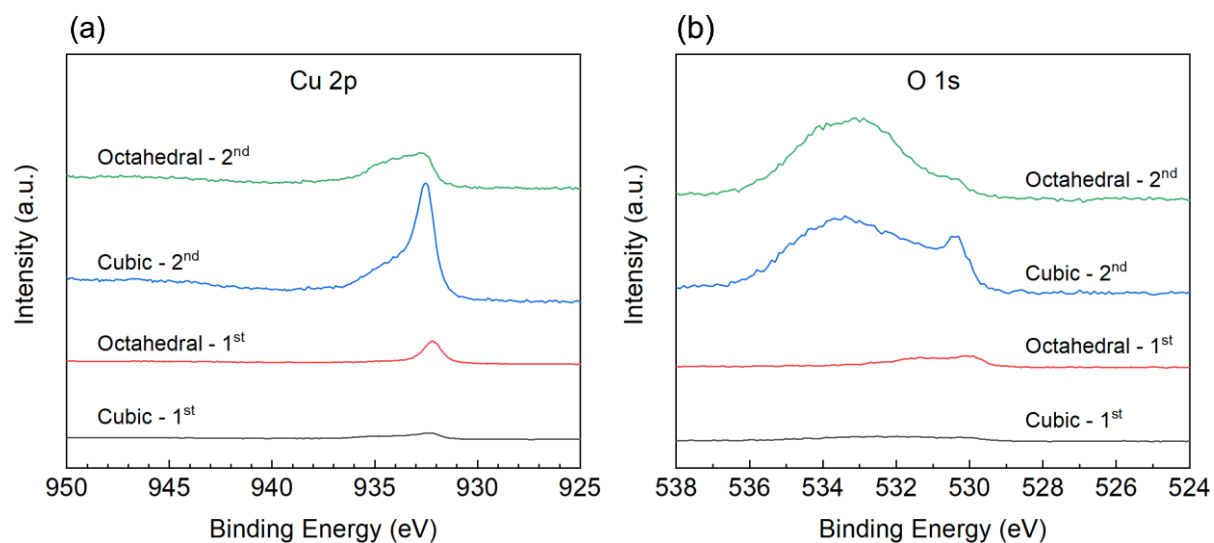
	0.6 sccm	0.7 sccm	0.8 sccm	0.9 sccm	1.0 sccm
0 h	43	11528	1190	42	15
6 h	1222	16934	-	35	17
12 h	6758	10680	334	46	19
24 h	13727	36305	251	46	19

Annex C



KPFM results: (a) topographic image and (b) contact potential difference map of a Cu_2O thin-film from the HP set deposited using a 0.7 sccm O_2 flow rate.

Annex D



XPS data from (a) Cu 2p and (b) O 1s emissions relative to cubic and octahedral particles obtained in 1st and 2nd syntheses.